1004

A169492

AD A169 492

R and D CENTER

LABORATORY

TECHNICAL REPORT

NO. 13109

ION ACOUSTIC MICROSCOPY

CONTRACT NUMBER DAAE07-83-M-R045

July 1985

K. O. Legg
Georgia Tech University
Atlanta, GA 30332

D. N. Rose
US Army Tk-Autmv Command
ATTN: AMSTA-ZSA
Warren, MI 48397-5000

by

Distribution Unlimited; Available for Public Release

U.S. ARMY TANK-AUTOMOTIVE COMMAND
RESEARCH AND DEVELOPMENT CENTER
Warren, Michigan 48397-5000

NOTICES

This report is not to be construed as an official Department of the Army position.

Mention of any trade names or manufacturers in this report shall not be construed as an official indorsement or approval of such products or companies by the US Government.

Destroy this report when it is no longer needed. Do not return it to the originator.

UNCLASSIFIED
SECURITY CLASSIFICATION OF THIS PAGE

REPORT DOCUMENTATION PAGE

1a. REPORT SECURITY CLASSIFICATION UNCLASSIFIED	1b. RESTRICTIVE MARKINGS NONE
2a. SECURITY CLASSIFICATION AUTHORITY	3. DISTRIBUTION/AVAILABILITY OF REPORT Approved for Public Release Distribution Unlimited
2b. DECLASSIFICATION/DOWNGRADING SCHEDULE	
4. PERFORMING ORGANIZATION REPORT NUMBER(S)	5. MONITORING ORGANIZATION REPORT NUMBER(S)
6a. NAME OF PERFORMING ORGANIZATION Georgia Tech Research Corp. 6b. OFFICE SYMBOL (If applicable)	7a. NAME OF MONITORING ORGANIZATION US Army Tk-Autmv Command
6c. ADDRESS (City, State, and ZIP Code) Georgia Institute of Technology Administration Building Atlanta, GA 30332	7b. ADDRESS (City, State, and ZIP Code) RDE Center ATTN: AMSTA-RSA Warren, MI 48397-5000
8a. NAME OF FUNDING/SPONSORING ORGANIZATION 8b. OFFICE SYMBOL (If applicable)	9. PROCUREMENT INSTRUMENT IDENTIFICATION NUMBER DAAE07-83- M-R045
8c. ADDRESS (City, State, and ZIP Code)	10. SOURCE OF FUNDING NUMBERS PROGRAM ELEMENT NO. / PROJECT NO. / TASK NO. / WORK UNIT ACCESSION NO.

11. TITLE (Include Security Classification)
Ion Acoustic Microscopy

12. PERSONAL AUTHOR(S)
Keith O. Legg Douglas N. Rose

13a. TYPE OF REPORT	13b. TIME COVERED	14. DATE OF REPORT (Year, Month, Day)	15. PAGE COUNT
Final Report	FROM Jul 83 TO Jun 84	1985, July, 01	25

16. SUPPLEMENTARY NOTATION The views, opinions, and/or findings contained in this report are those of the authors and should not be construed as an official Department of the Army position, policy, or decision, unless so designated by other documentation.

17. COSATI CODES			18. SUBJECT TERMS (Continue on reverse if necessary and identify by block number)
FIELD	GROUP	SUB-GROUP	Ion Acoustic Microscopy, Photoacoustic Microscopy, Thermal Wave Imaging, Zirconia, Ion Implantation

19. ABSTRACT (Continue on reverse if necessary and identify by block number)
This report details the modifications to an existing ion implanter which were made in order to use it for ion acoustic microscopy. Results are described of tests of the technique on samples of cubic zirconia impanted with nitrogen ions. The utiltiy of the technique for monitoring the progress of implantation in metals and ceramics is discussed.

20. DISTRIBUTION/AVAILABILITY OF ABSTRACT ☒ UNCLASSIFIED/UNLIMITED ☐ SAME AS RPT. ☐ DTIC USERS	21. ABSTRACT SECURITY CLASSIFICATION UNCLASSIFIED
22a. NAME OF RESPONSIBLE INDIVIDUAL DOUGLAS ROSE	22b. TELEPHONE (Include Area Code) (313) 574-7752 22c. OFFICE SYMBOL AMSTA-RSA

DD FORM 1473, 84 MAR 83 APR edition may be used until exhausted. All other editions are obsolete.

SECURITY CLASSIFICATION OF THIS PAGE
UNCLASSIFIED

TABLE OF CONTENTS

Section		Page
1.0.	INTRODUCTION	5
2.0.	EQUIPMENT	6
3.0.	EXPERIMENTAL RESULTS	8
3.1.	Implanter Operation	8
3.2.	Signal Detection	8
3.3.	Changes In Acoustic Signals On Implantation	8
4.0.	THEORETICAL MODELING	10
5.0.	DISCUSSION	20
5.1.	Equipment	20
5.2.	IAM Images	20
5.3.	Comparison With Photoacoustic Microscopy	21
6.0	USEFULNESS AND APPLICATIONS OF IAM	22
LIST OF REFERENCES		24
DISTRIBUTION LIST		Dist-1

LIST OF ILLUSTRATIONS

Figure	Title	Page
2-1.	Standard Implanter (lower labels) And Modifications (upper labels).	7
3-1.	Acoustic Signals During Implantation Of Cubic Zirconia	9
3-2.	a) IAM Image Of N_2+ Implanted Zirconia - In-Phase Signal	11
	b) IAM Image Of N_2+ Implanted Zirconia - Quadrature Signal	12
3-3.	a) Video And Graphical IAM Images Of N_2+ Implanted Zirconia	13
	b) Inverse Video And Graphical IAM Images Of N_2+ Implanted Zirconia	14
3-4.	Optical Micrographs Of Surface Of Sample	
	a) Outside Implanted Region.	
	b) Periphery Of Implanted Spot	15
	c) Further Inside Implanted Region.	
	d) Further Inside Implanted Region	16
	e) Center Of Implanted Spot	17
4-1.	Thermal Skin Depth And Surface Temperature For Zirconia Under Harmonic Surface Heating	19

1.0. INTRODUCTION

The photoacoustic effect using ion beam excitation has been demonstrated in this work. Results of its use on zirconia are shown.

The photoacoustic effect was first reported by Alexander Graham Bell in 1880. There was considerable initial work, but, after a short time, the effect lay dormant for 50 years until the advent of improved microphones, when it was revived for work with gases. However, it was not reapplied to solids until 10 years ago [1], again upon the advent of a technological advance, the widespread availability of intense directed energy beams such as the laser. The first photoacoustic microscopy image was produced less than 6 years ago [2].

An early experiment of Bell's illustrates the photoacoustic effect well. He had a closed glass vessel to which a hearing tube was attached. There was solid material inside the glass vessel. When the glass vessel was illuminated with rapidly interrupted sunlight, a sound was heard at the interruption or modulation frequency. When the sunshine was stronger, the sound was stronger. Also, the sound was stronger when the solid material inside had a darker color. As we understand it today, the modulated light was absorbed at the surface of the material, producing a modulated temperature variation at the surface of the material. This, in turn, periodically heated the air above the surface producing periodic changes in the pressure of the air above the surface, i. e., sound, which could be detected by the ear.

The photoacoustic concept has now been considerably extended. It is realized that the periodic heating mentioned above generates a highly damped thermal wave which probes the thermal properties of the surface and near surface down to about 1 mm. This thermal wave probing gives photoacoustic microscopy its other name, thermal wave imaging. A variety of effects occur at the heated spot in addition to heating of the air above the spot. There are periodic variations of the infrared radiation from the spot and periodic expansions and contractions of the heated spot. This last produces a slight periodic bulging of the surface and generates acoustic waves into the solid. Detailed descriptions of thermal wave imaging and its potential for nondestructive evaluation are given in the literature [3-15].

The heating of the spot does not have to be by light. In our case, it is via an ion beam. There is a high vacuum inside an ion implanter, so obviously, we can not use detection of sound in the gas above the spot. We detect the acoustic waves in the solid sample itself.

2.0. EQUIPMENT

Modifications were made to the existing Accelerators Inc. 200 KeV ion implanter at Georgia Tech to allow it to be changed easily from normal ion implantation to scanning ion acoustic microscopy (IAM). This implanter is a standard semiconductor machine intended for research and has a hot cathode ion source, permitting it to generate beams of almost any ionic species. A schematic diagram of this equipment is shown in Fig. 2-1, which also indicates where modifications were made. When it is operating in its normal implantation mode, ions are generated from a plasma in the source, from which they are extracted, focused and accelerated to the desired energy. They are then refocused through a magnet and aperture slit to accomplish separation by charge/mass ratio. The mass-separated beam is refocused and directed through a neutral beam dump (to remove neutrals, which contribute to the dose but not to the measured beam current) onto the sample. The beam may be scanned over the sample if necessary to ensure a uniform implant.

In order to permit IAM operation, modifications were made as shown schematically in Fig 2-1. Vertical scanning plates were added immediately before the analyzing magnet, together with a 0.5 mm or 2 mm diameter aperture in a movable plate placed directly behind the normal slit aperture. A sinusoidal voltage of up to 50 V peak-peak on the plates scanned the beam across the aperture to produce a 10-20% variation in beam current passing through the aperture. To aid in focusing and positioning the beam, the existing beam monitor flap in front of the sample was modified to incorporate a Faraday cup with a 1.6 mm diameter aperture. By scanning the beam and sending a portion of the scanning voltages to the X and Y inputs of an oscilloscope, with a signal proportional to the Faraday cup current going to the Z (intensity) axis, it was possible to obtain an image of the beam spot. The shape and position of the beam could then be adjusted with the quadrupole lenses to provide a well-focused, properly positioned beam.

The scan drive was modified to permit the scanning plates to be driven by a PDP-8 computer interfaced to a set of programmable high voltage power supplies. Programming was designed to scan the beam alternately up and down across the sample in a series of 48 vertical lines. Each line was divided into 48 points, at each of which the beam was stopped to permit the acoustic signal to be recorded.

The acoustic signal detector is also shown in Fig. 2-1. It consists of a conical block with the sample glued onto the large end with cyanoacrylate glue and a capacitance microphone affixed to the other. The block was machined out of aluminum. Its shape was designed to transmit the sound while amplifying its intensity [16].

All work was carried out on single crystal cubic zirconia both because it is a well-defined material and because we already have a fairly extensive knowledge of its behavior under ion implantation. Furthermore, cubic zirconia has been prominently employed in the Cummins adiabatic diesel program.

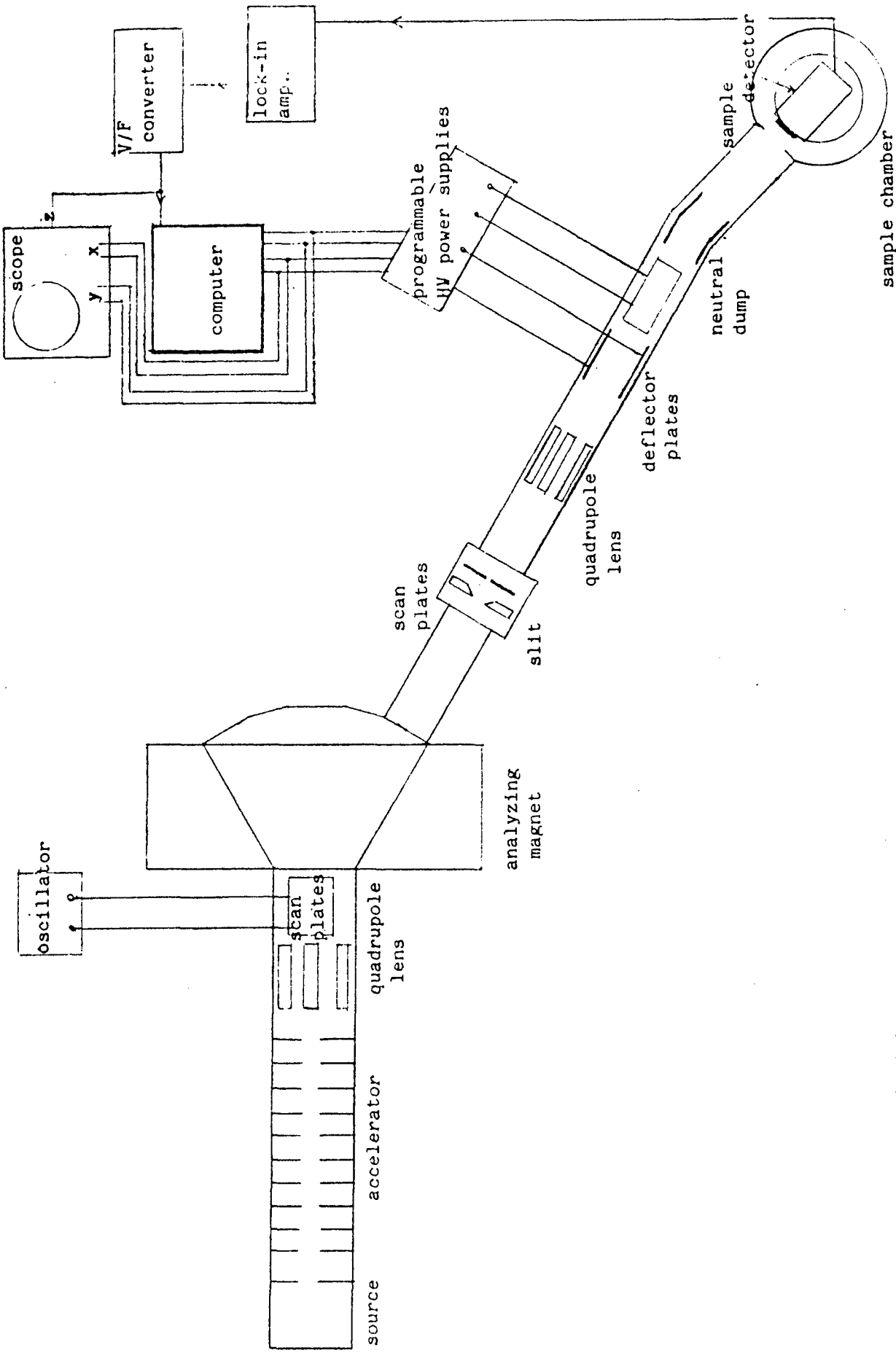

Fig 2-1. Standard Implanter (lower labels) And Modifications (upper labels)

3.0. EXPERIMENTAL RESULTS

3.1. Implanter Operation

It had been hoped that it would be possible to focus the beam to a size of approximately 1 mm diameter at the sample to provide fine spatial resolution and a large beam power density. In fact, the characteristics of the implanter permitted focusing to this size beam only in one direction. Thus a beam with dimensions of 1 mm in one direction measured 1 cm or more in the other. In practice, circular beams of the order of half a centimeter diameter were usually obtained. However, the spatial resolution was in reality somewhat better than this since the beam shape was generally close to Gaussian, as determined by moving the beam across the aperture in the beam plate Faraday cup and recording the measured current at each position.

With a 50 V peak-peak sine wave applied to the chopper plates, the sinusoidal variation in the chopped beam current was generally 10-20% on a total beam current of 1 to 10 microamps. For a 100 KeV beam with a 6 mm diameter spot, this translates to a harmonic power density of 0.04 - 0.7 Watts/sq. cm. at the center of the spot.

A finely focused spot at the specimen would require a high brightness ion source which could be imaged onto the sample surface. In an attempt to achieve this, a Capillaritron source [17] was installed and tested on the machine. It was found, however, to be unsuitable for this type of implanter since its efficiency (in terms of ions generated per atom supplied) was 1% or less. This led to a large gas flow, which raised the pressure in the source area beam line above 10^{-4} Torr. At this pressure, the beam was almost completely neutralized before reaching the magnet, leaving almost no ion current at the sample.

3.2. Signal Detection

In our initial work [18] we had used a piezoelectric transducer. To check alternatives, we used a capacitance microphone. While this was adequate for signal pick-up, its sensitivity rolled off badly above 8 kHz, restricting our work to 6 kHz or less. Signal levels at the lock-in detector input were generally in the range 1-25 mV, similar to those which were obtained in our initial study using a piezoelectric transducer bonded directly to the sample.

3.3. Changes In Acoustic Signals On Implantation

The response of the system to changes in surface properties brought about by implantation is illustrated in Fig. 3-1. The sample was implanted with 100 KeV N_2^+ ions through a 6 mm diameter aperture, using a beam swept across the aperture by the chopper plates. At the same time, the acoustic signal at the chopping frequency was measured to monitor changes as the implantation

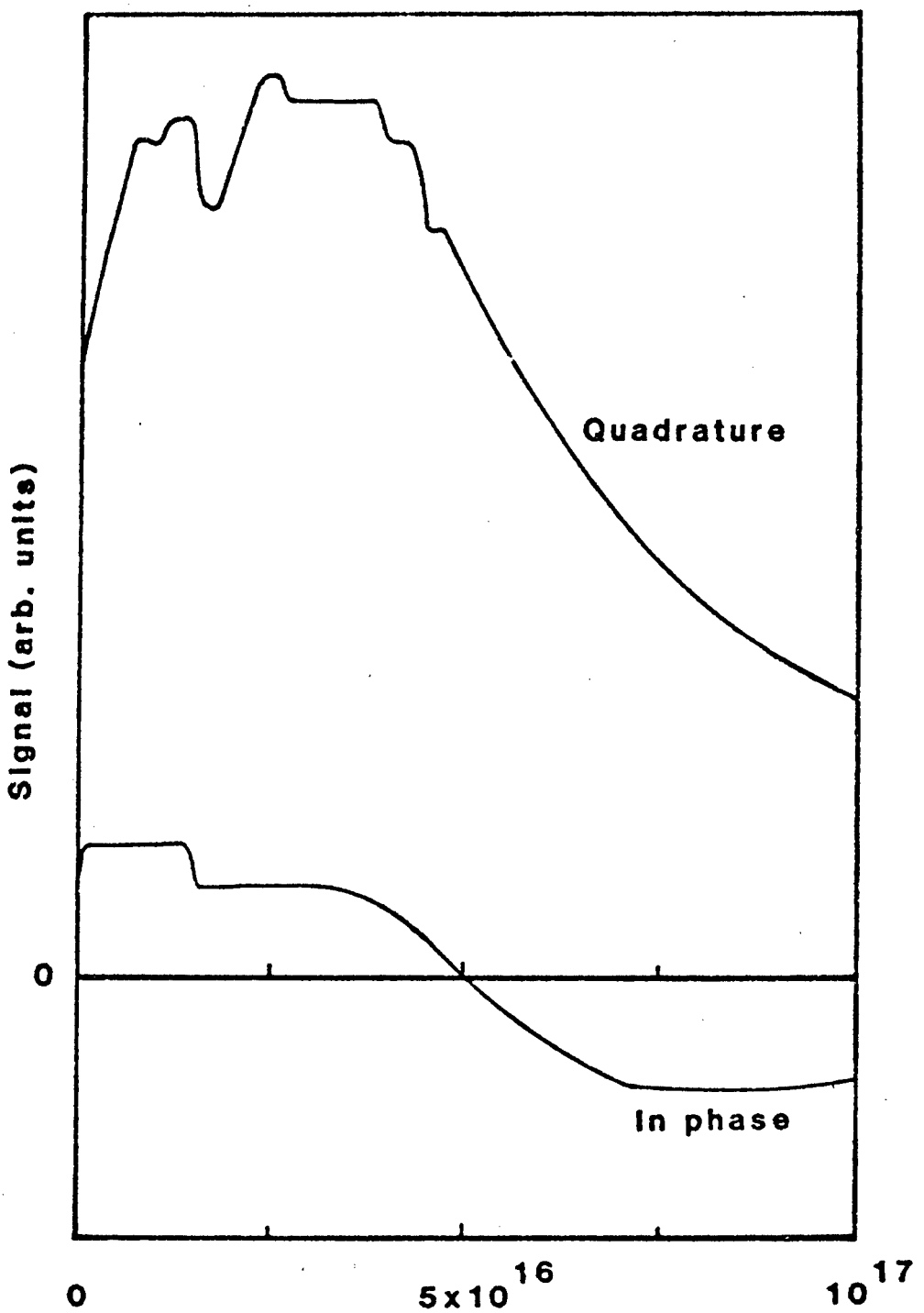

Figure 3-1. Acoustic Signals During Implantation of Cubic Zirconia

proceeded. Both the in-phase and quadrature signals were recorded simultaneously. These signals represent the average changes over the whole implant area. The initial rise in the signals is due to heating of the sample and is always seen in IAM. The changes below 2×10^{16} are probably due to variations in beam current density. At 3×10^{16} N_2 ions/sq cm (6×10^{16} N/sq cm) the surface begins to blister due to lattice strain [19]. At this point the acoustic signal begins to drop, and as the dose rises further the quadrature signal even changes sign. When a dose of 10^{17} ion/sq cm had been reached, implantation was stopped and an IAM image was generated of the entire crystal including the implanted spot. This IAM image is shown in Fig. 3-2, where the image is plotted in perspective with the signal intensity as the z-axis. Fig. 3-3 shows the same images in both video and inverse video as well as in another graphical form. However, in Fig. 3-3, the artifact signals arising from impact of the ion beam outside the crystal on the aluminum support have been removed through image processing.

In order to relate the acoustic signals to changes in the surface, optical micrographs were taken across the interface between the unimplanted and implanted regions of the crystal. These are shown in Fig. 3-4. The unimplanted region shows a smooth surface with only scratches remaining from polishing evident (Fig. 3-4a). Blisters become evident in the "penumbra" region around the periphery of the implanted area (Fig. 3-4b), which received a lower dose than the central region. These become more numerous as the dose increases further within the implanted spot (Fig. 3-4c). In the regions further from the outside of the spot, which had received a still higher dose, the blisters have disappeared, probably because they have coalesced (Fig. 3-4d). In some areas, cracking of the surface had occurred, as evidenced by an arc of light colored spots (Fig. 3-4d). Finally, completely inside the implanted area, there is no evidence at all of blistering (Fig. 3-4e).

4.0. THEORETICAL MODELING

It is possible to describe the periodic heating and cooling of the surface region by a sinusoidal heat source in terms of purely classical heat transport. Since the beam only penetrates (and so deposits energy) to a depth of about 0.1 microns, while significant changes in temperature take place over several microns, the heat source can be considered to be in the surface plane. The situation then reduces to the classical problem which has been analyzed in the literature [20,21]. Based on this classical analysis, computer programs have been set up to calculate the response of a solid to sinusoidal and square wave heat sources. The general nature of this response is most easily seen in thinking of the surface temperature produced at a zirconia surface by a square

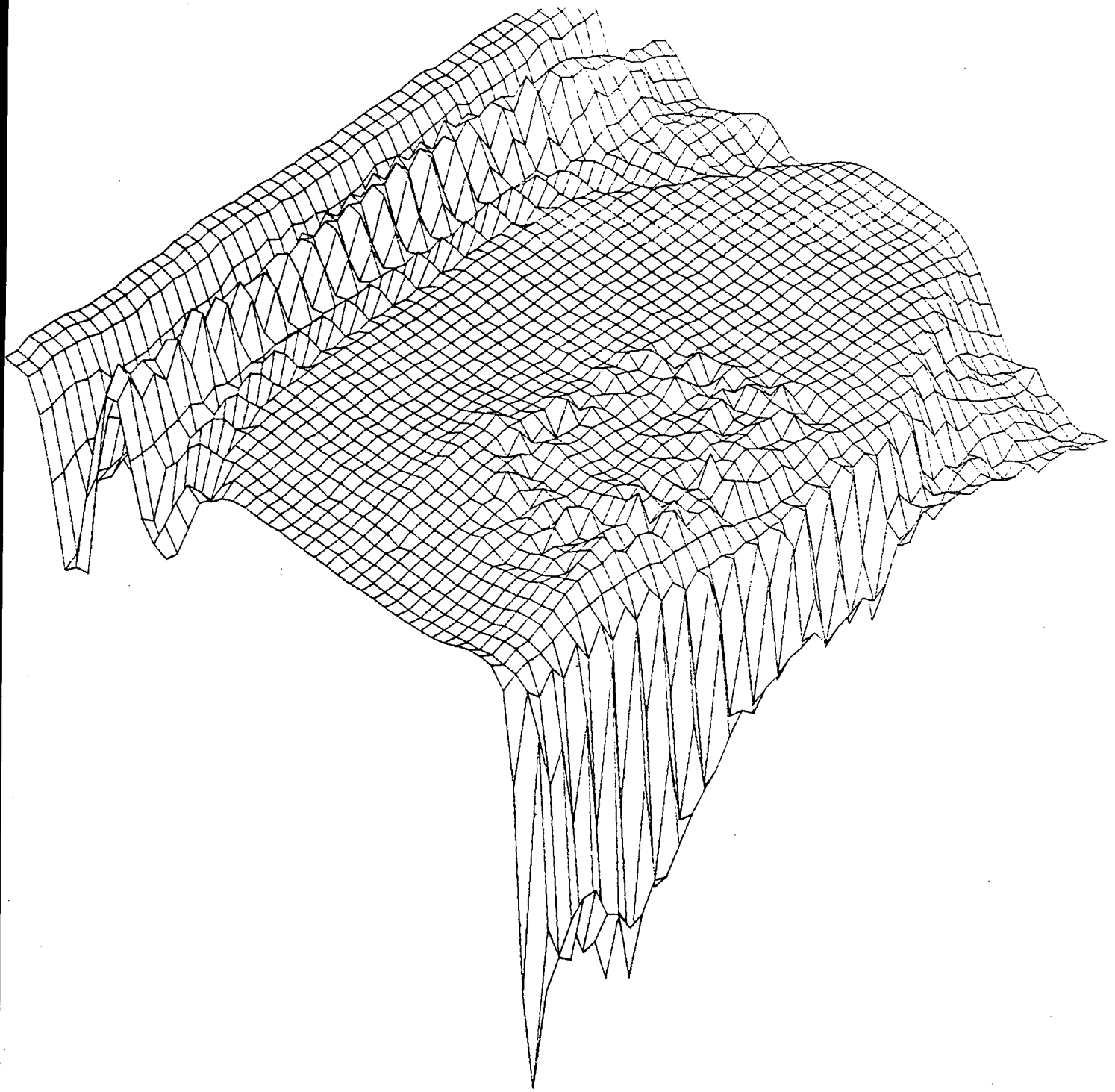

Figure 3-2. a) IAM Image of N_2^+ Implanted Zirconia - In Phase Signal

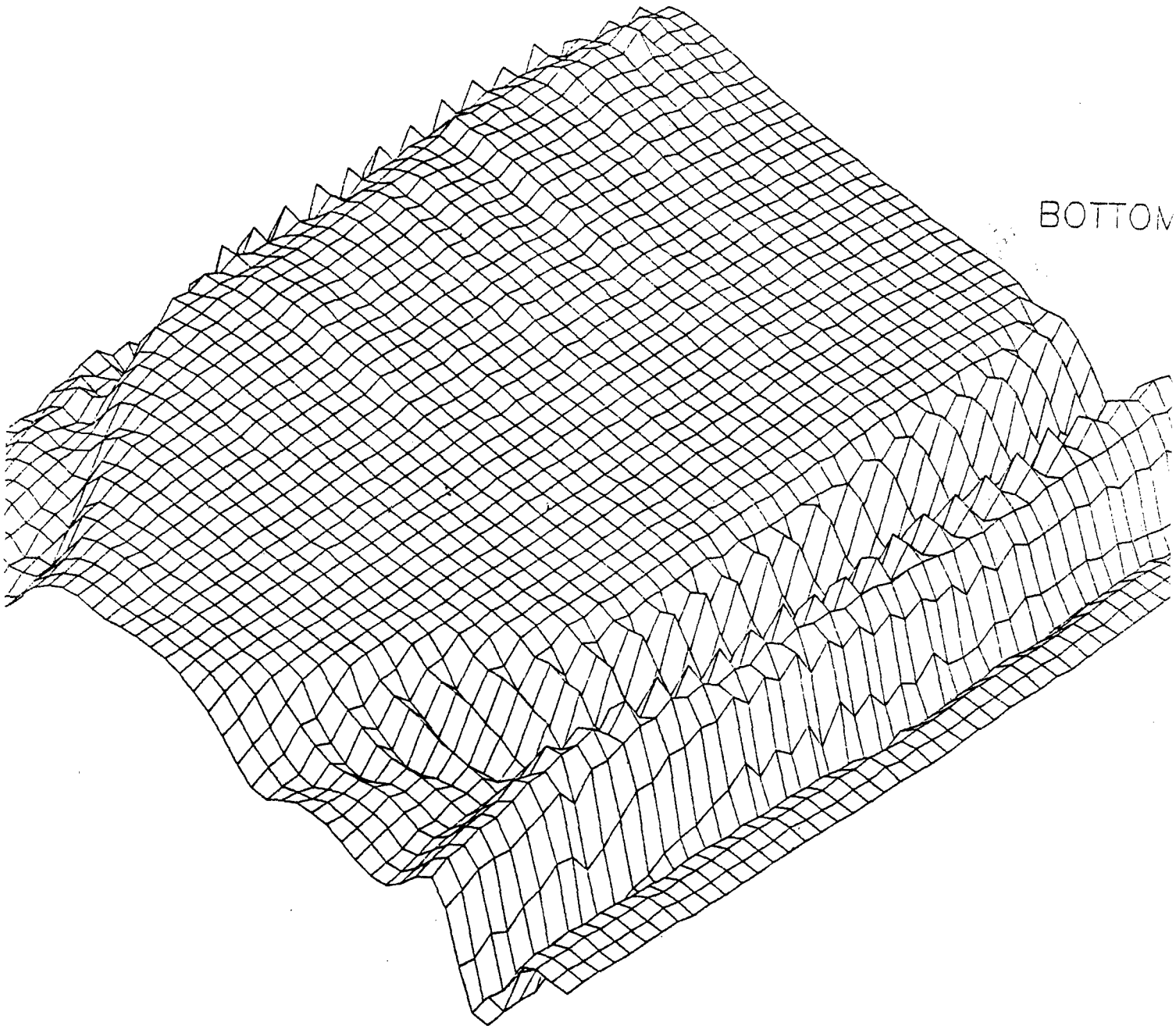

Figure 3-2. b) IAM Image of N_2^+ Implanted Zirconia - Quadrature Signal

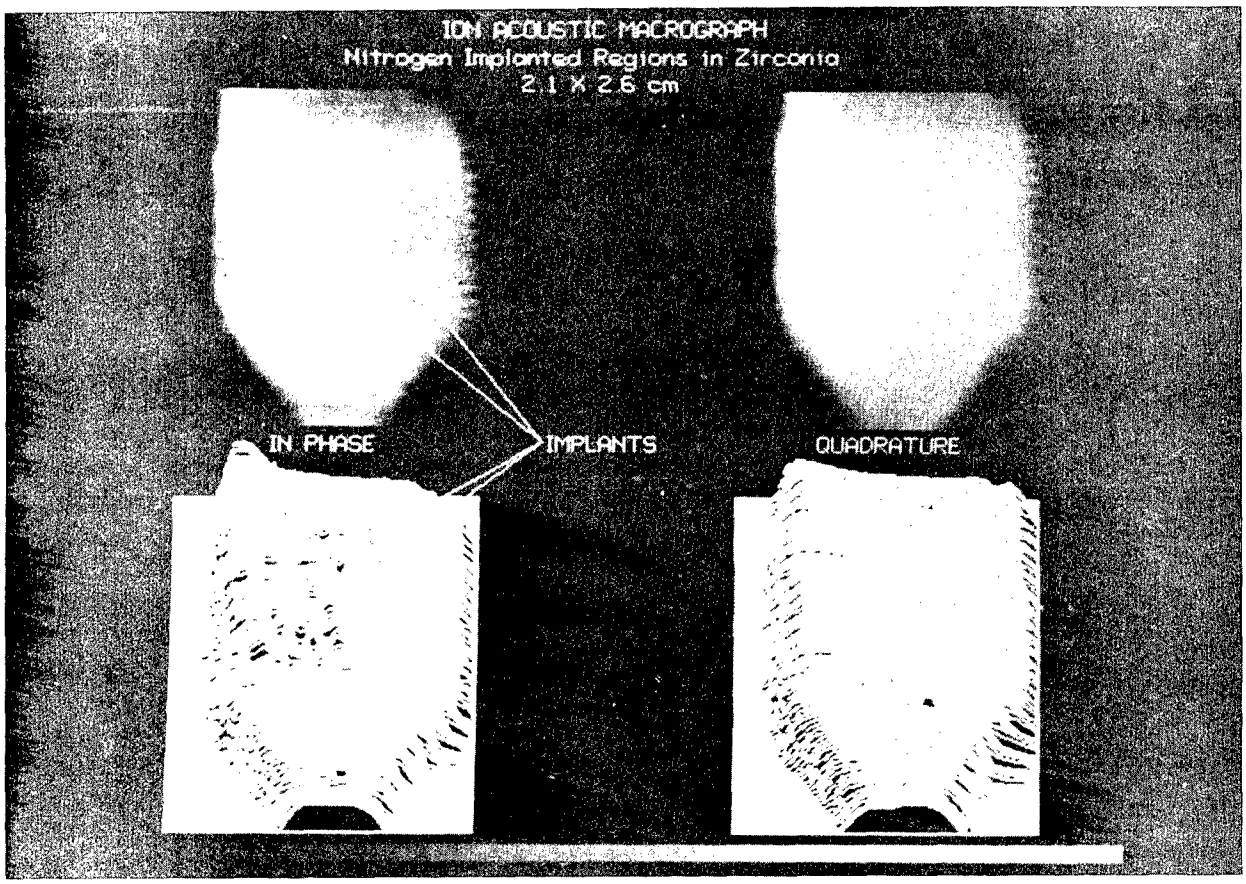

Figure 3-3. a) Video and Graphical IAM Images of N_2^+ Implanted Zirconia

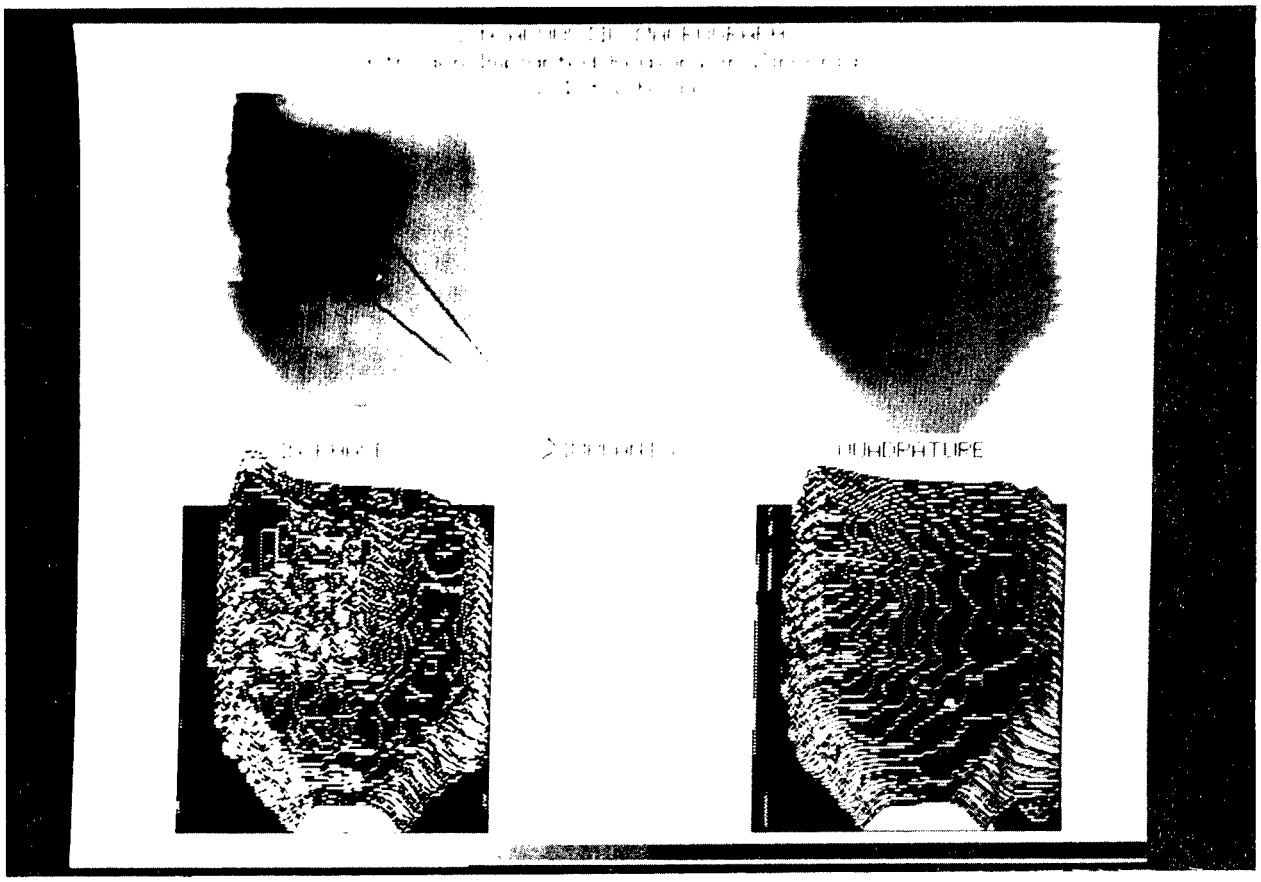

Figure 3-3. b) Inverse Video and Graphical IAM Images of N_2^+ Implanted Zirconia

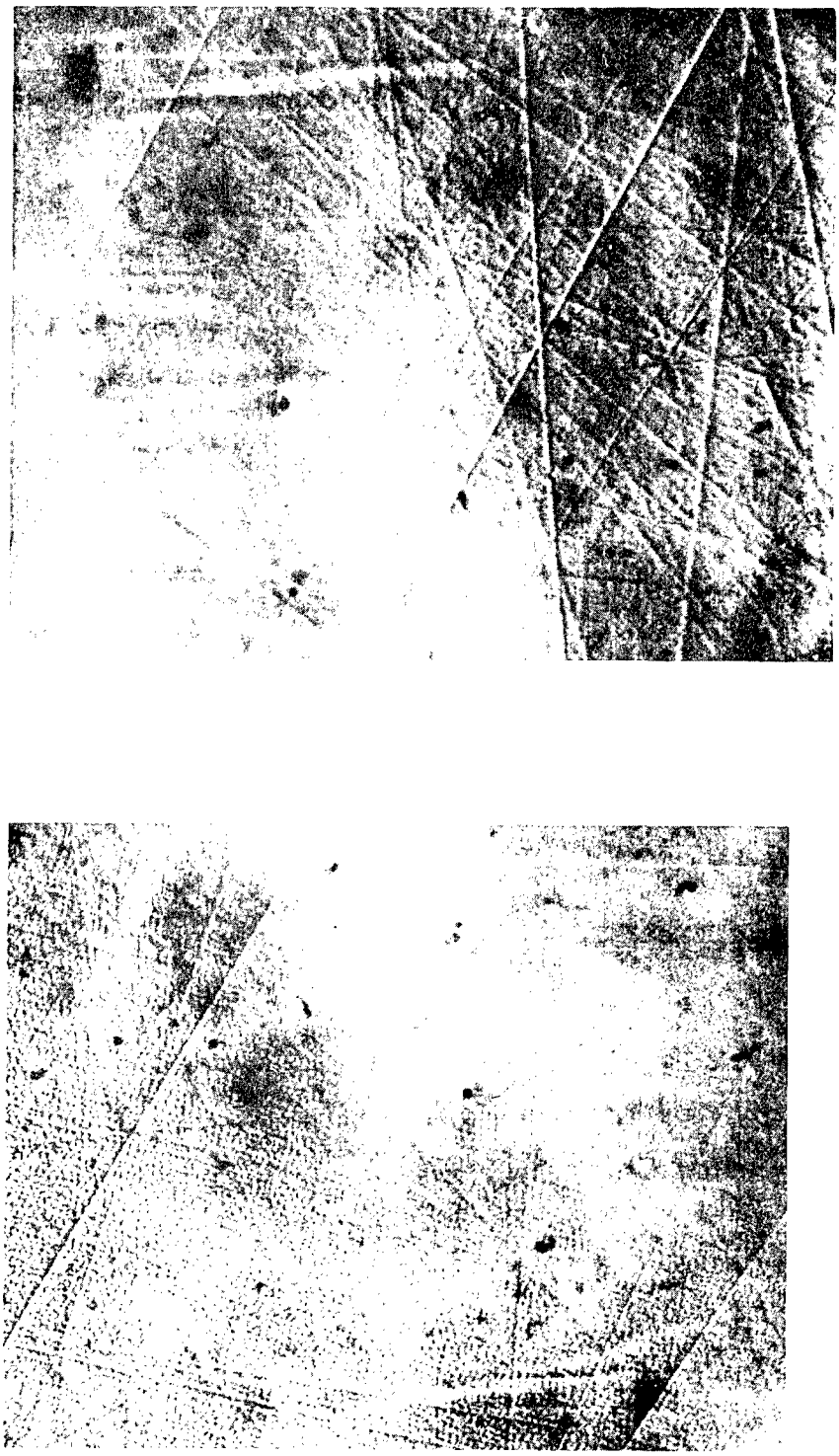

Figure 3-4. Optical Micrographs of Surface of Sample
a) Outside of Implanted Region
b) Periphery of Implanted Spot

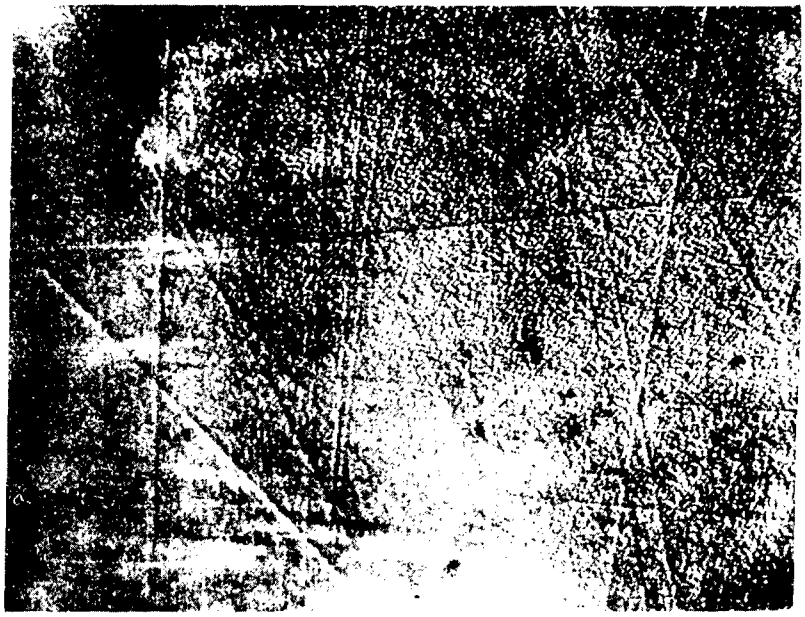

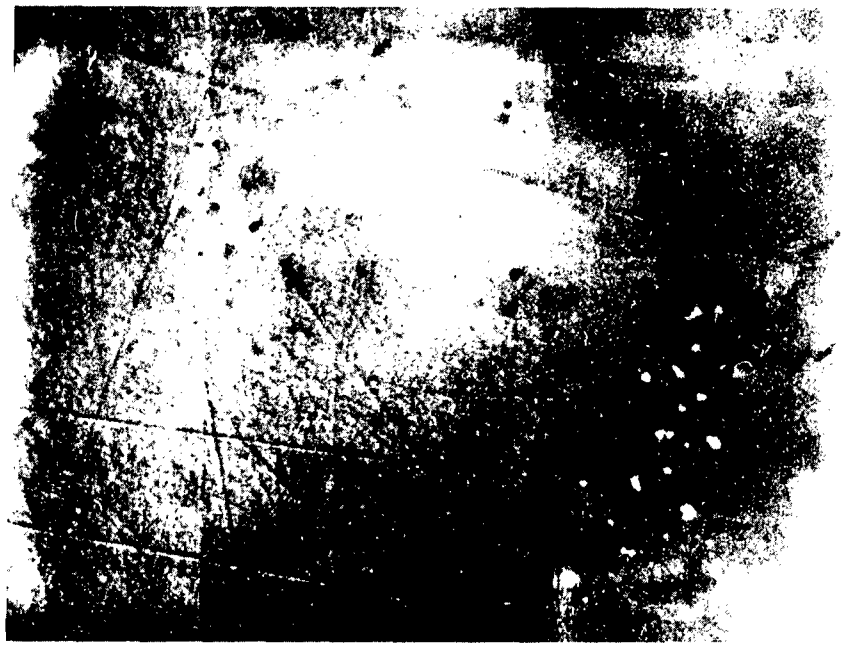

Figure 3-4. Optical Micrographs of Surface of Sample
c) Further Inside Implanted Region
d) Further Inside Implanted Region

Figure 3-4. Optical Micrograph of Surface of Sample
e) Center of Implanted Spot

wave heat source. The surface temperature rises while the heat source is active and falls thereafter, but not to its original value, leading to a general heating of the material. Also, since the surface temperature is rising during all of the heating phase, its peak value generally lags the time when the heat input begins and hence it will be retarded in phase from the heat source. For IAM, in which an approximately sinusoidal heat source is used, a highly damped sinusoidal thermal wave is produced which has a characteristic skin depth, d, called the thermal diffusion length. Over this distance the thermal wave amplitude drops to 37% of its initial value. It is defined as follows:

$$d = (2K/wpC)^{1/2}$$

where

K = thermal conductivity

p = density

C = specific heat

w = $2\pi f$, with f = modulation frequency.

In practice this skin depth is usually of the order of microns - far greater than the implantation depth. This justifies the assumption of a surface heat source for all but the highest frequencies.

For a harmonic heat source of the form

$$P = P_o \exp(iwt)$$

where

P = power density,

the harmonic temperature amplitude at depth x is given by:

$$T_{harm} = P_o (1/wpKC)^{1/2} \exp(-x[wpC/2K]^{1/2}).$$

Fig. 4-1 shows calculated values of the skin depth and surface harmonic temperature for thermal wave generation in zirconia. As can be seen in Fig. 4-1, the implantation depth does not equal the skin depth until about 10 MHz. Until this frequency, the thermal response includes interaction of the thermal wave with material lying considerably below the implantation zone. However, if the modulation frequency is raised, the temperature excursions decrease as can also be seen in Fig. 4-1. For example, even for a 20 Watt/cm^2 beam, the surface temperature excursion is only about 0.1 degrees C at a frequency of 3 kHz. Since we had a smaller beam power and since this temperature amplitude is proportional to beam power, it would have been about .0035 degrees C for this work.

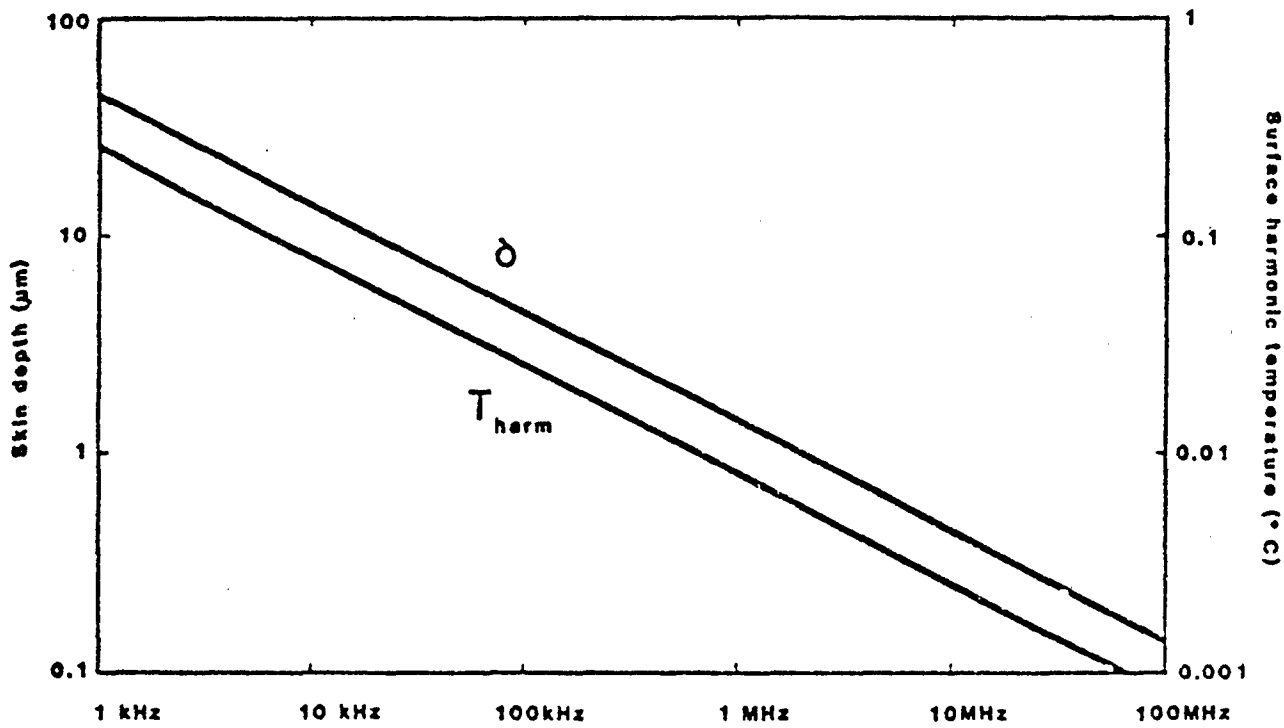

Figure 4-1. Thermal Skin Depth and Surface Temperature for Zirconia Under Harmonic Surface Heating

5.0. DISCUSSION

5.1. Equipment

Signal generation

5.1.1. Signal Generation. Since the implanter was not designed for this type of work its use in this application is somewhat difficult, but not impossible, as can be seen from the results. In order to generate an IAM image, the machine had to operate stably. This usually required several hours of continuous operation. Because of the type of source and the focusing lenses used, focusing was very difficult. The problems of getting a beam which was focused were eased by the addition of a small-aperture Faraday cup to the beam monitor plate, but it was found to be impossible to get a circular spot less than about 6 mm in diameter. This would at first appear to limit the spatial resolution of the technique to this value. However, since the beam intensity across its diameter is usually roughly Gaussian, the strongest acoustic signals come from the center of the beam spot on the sample. Thus in practice the spatial resolution is better than 6 mm, as can be seen from Figs. 3-2 and 3-3.

5.1.2. Signal Detection. Detection of the acoustic signals involves generating the signals at the sample surface, propagating them though the material, coupling them into the aluminum cone, transferring them down the cone, coupling them into the microphone element and finally measuring the electrical signal. Clearly, generation and propagation of the signals depends on surface condition and thus embodies what we wish to measure. Cyanoacrylate glue was used to couple the sample to the cone and the cone to the microphone. This appeared to be a reasonable vacuum-compatible material, but may not have been the best choice. The cone design could be improved to make it more closely resemble a typical acoustic horn, but this would be far more difficult to make. The cone was used to try to eliminate any dependence of the signal on its point of generation across the sample surface, though better acoustic impedance matching may be obtained by gluing the sample directly to the transducer, depending on the sample and microphone. Finally the microphone itself could be better replaced by a piezoelectric transducer. This would permit operation at frequencies in the megahertz range.

5.2. IAM Images

In Figs. 3-2 and 3-3 the edges of the sample can be clearly seen. The implanted area is visible as a region of more intense acoustic emission which appears only in the in-phase component. The region within the spot shows somewhat variable acoustic intensity. According to theoretical estimates based solely on thermal wavelength, it should not be possible to record changes in surface thermal properties on a depth scale less than about 10 microns for this frequency, while the implant depth is only about 0.1 microns. However, consideration of the volume into which the energy is deposited and from which the thermal and acoustic waves propagate into the solid is the other part of resolution in thermal microscopies so that our observations are in good agreement with current theory [22].

It can be seen in Fig. 3-2 and Fig. 3-3 that the highest contrast between the signal from the implanted region and the rest of the crystal is at the periphery of the implanted region which is also the region where blisters are observed. The skin of the blisters is separated from the underlying material and previous work [19] has shown that the skin of these blisters has a thickness equal to the penetration depth of the ions which is about twice the projected range. We assume that the blisters, being due to built up strain in the lattice, are empty. Then heat and acoustic waves from beam power deposited in the skin of the blister could not propagate directly into the bulk. In this case, we would expect the thermal response to drop significantly in the blistered area, which is opposite to the observed result. Of course, heat generated in the skin of a blister can flow sideways into the surrounding area, leading to a larger than normal increase in temperature there but this should merely create an extra heat source in the surface between the blisters with no net effect on the acoustic emission.

There is the possibility that the blisters were bubbles of gas under high pressure, such as those often seen in heavily irradiated materials. This could act as a barrier to heat diffusion while permitting acoustic wave propagation. This would lead to far higher temperature variations over the blisters but it would seem that this would merely cause thermal expansion of the skin of the blisters, which would make them bulge outward more, lowering the pressure inside of themselves and creating an acoustic wave in antiphase with the waves generated elsewhere on the surface. Again this is opposite to what is observed. However, flexing of the skin of the blister would create mechanical strains in the surrounding surface, with or without the presence of gas. This would produce shear waves which would couple into the bulk of the crystal and thence into the acoustic transmission system as a combination of shear and compressive waves.

The condition of the surface in the fully implanted center of the spot is not known. The most likely possibilities are that either the surface region has split off entirely (as we have seen to happen in other cases), or the blisters have coalesced and their skin collapsed onto the substrate. In either case fairly normal acoustic and thermal wave generation and propagation would again be possible.

From the foregoing discussion it is evident that much remains to be understood; however, we are able to detect the onset of blistering, and probably other forms of severe surface distortion, even at low frequencies. We have also been able to generate images of reasonable resolution even with rather broad ion beams.

5.3. Comparison With Photoacoustic Microscopy

The thermal and acoustic waves arising in both approaches will behave the same once they are generated. Basic differences arise because the energy deposition mechanisms are different. With laser generation, the phenomena is optical absorption, which has a decreasing exponential profile with the most energy being deposited at the surface. On the other hand, because of the statistical nature of ion stopping, their energy is lost in a Gaussian profile with most of

the energy being deposited a few tens of nanometers beneath the surface typically with an ion implanter or a few nanometers in the case of SIMS. The difference between optical absorption and ion stopping is illustrated dramatically for optically transparent materials. The implanted areas in the zirconia single crystal slabs are clearly imaged by IAM but were invisible using the current TACOM photoacoustic system. The optical absorption of materials varies widely whereas, for comparison, there are no ion transparent materials. With laser generation, there can be photochemical effects. With ion beam generation, some modification of the surface chemistry and stresses is unavoidable as ions are stuffed into the surface.

Ultimate resolutions of thermal microscopies are a function of both the smallest spot size attainable and the highest reasonably attainable modulation frequencies [22]. For ion beam generation using a secondary ion mass spectrometry (SIMS) approach [23], the smallest spot size is about 10 microns. For Ar ion laser generation, the smallest spot size is about 1 micron, which is approximately 2 light wavelengths. [Making a play on words, but emphasizing a possible nomenclature confusion for some, we can compare a beam of Ar ions such as can be used in an implanter or SIMS, and the light from excited Ar ions, as from an Ar ion laser, by whimsically saying "an Ar ion beam will give you 1 while a beam of Ar ions will only give you 10".] For a typical ion implanter,as used in this study, the spot size is several millimeters. For our uses here, the spot size can be thought of as determining the lateral resolution while the modulation frequency can be thought of as determining the depth of sampling. The highest attainable modulation frequency now is determined by signal detection method frequency limitations rather than beam modulation capabilities. Since any vacuum compatible signal detection method used with laser beam generation can be used with ion beam generation, the depth of sampling can be the same with either technique.

A big practical difference is that ion beam generation requires a vacuum environment whereas laser generation does not. Thus laser beam generation has a much wider general area of application. However, for utilizing the photoacoustic technique for real time monitoring of ion beam processing, it is much more straight forward to modulate the ion beam directly rather than to bring in the complexities associated with implementing an auxiliary modulated laser to excite a photoacoustic effect.

6.0. USEFULNESS AND APPLICATIONS OF IAM

In order to attain the spatial resolution which is possible with photoacoustic microscopy, extensive modifications would have to be made to any standard commercial ion implanter. This would clearly render the technique of little use as a monitor of the implantation process as it is usually carried out. However, to monitor the progress of an implant it would seldom be necessary to have a spatial resolution better than, say, a quarter of an inch, since one would be seeking to observe changes in the acoustic signals in various sample areas rather than to image the sample itself. In order for the technique to be technologically useful it must be possible to generate and detect the acoustic signals in a straightforward manner while scanning the beam across the part being implanted. As we have demonstrated, the beam can be modulated quite

easily by scanning it across a small aperture. The problem with this technique is that it makes the transmitted beam current strongly dependent on the beam position. It also reduces the overall beam current if the aperture is smaller than the beam. Both these problems can be overcome by using an aperture slightly larger than the beam diameter. Alternatively, modulation could be effected at the source, by modulating the extractor, for example. Another alternative is coordinate modulation [24] which has the considerable advantage that full beam power could be used continually and thus the production rate could remain the same.

In order to detect the acoustic signals, it is simplest to attach a transducer to the sample. Although this limits the freedom of sample movement, it need not necessarily be a serious problem. For example, the rotation needed to implant cylindrical samples could be 180 degrees in each direction, rather than being continuous. The presence of a transducer, together with its bonding glue, also limits the temperatures which the sample can be permitted to attain during implantation. This would in turn limit the allowable beam current density. For many of the implants which are likely to be used commercially in ceramics (Al, Zr etc.) this would not be a serious restriction. It would, however, reduce the efficiency with which one could implant high-current ions such as nitrogen. If the transducer and its glue could withstand temperatures in the region of 150 C even these implants would not generally be impaired. Again, as an alternative, another detection approach, such as interferometry [12], could be used to detect the acoustic wave.

From the data of Fig. 3-2 it is evident that the metal substrate also generates intense acoustic signals. Thus it is expected that the technique would find application in the area of metal implantation also. As we have discussed, in the ceramics the detection of the onset of blistering serves to indicate when the implant has reached too high a density locally. In metals, however, blistering seldom occurs except at very high dose [25]. In order to see changes occurring at lower doses it would be necessary to use modulation frequencies in the MHz range (see Fig. 4-1). It would in any case be advantageous to use such frequencies to attain a reasonable degree of surface sensitivity to monitor the changes in surface mechanical properties being imparted by the implant.

With a reasonably intense ion beam of 1 cm diameter or less, modulated at MHz frequencies, which can be scanned over the sample, IAM appears to be a viable method for monitoring the progress of implantation in metals and ceramics. It would appear to be applicable to implants made in most standard semiconductor-type implanters, which are most often used for this type of work.

LIST OF REFERENCES

(1) A. Rosencwaig, "History of Photoacoustics", Chapter 2 in Photoacoustics and Photoacoustic Spectroscopy, John Wiley and Sons, New York, New York (1980)

(2) Y. H. Wong, R. L. Thomas and G. F. Hawkins, "Surface and Subsurface Structure of Solids by Laser Photoacoustic Spectroscopy", Appl. Phys. Lett. 32, 538 (1978)

(3) J. A. Noonan and D. M. Munroe, "What is Photoacoustic Spectroscopy", Optical Spectra, February (1979)

(4) D. N. Rose, "Photoacoustic Microscopy - An Emerging Tool", p201, Proceedings of the 32nd Defense Conference on Nondestructive Testing, 1-3 November 1983, Wright Patterson Air Force Base, Oh[B

(5) R. L. Thomas, J. J. Pouch, Y. H. Wong, L. D. Favro, P. K. Kuo and A. Rosencwaig, " Subsurface Flaw Detection in Metals by Photoacoustic Microscopy", J. Appl. Phys. 51, 1152 (1980)

(6) P. K. Kuo, L. D. Favro, L. J. Inglehart, R. L. Thomas and M. Srinivasan, "Photoacoustic Phase Signatures of Closed Cracks", J. Appl. Phys. 53, 1258 (1982)

(7) A. C. Boccara, D. Fournier and J. Badoz, "Thermo-optical Spectroscopy: Detection by the Mirage Effect", Appl. Phys. Lett., 36, 130 (1980); A. C. Boccara, D. Fournier, N. Jackson and N. Amer, "Sensitive Photothermal Deflection Technique for Measuring Absorption in Optically Thin Media", Opt. Lett. 5, 377 (1980)

(8) J. C. Murphy and L. C. Aamodt, "Signal Enhancement in Photothermal Imaging Produced by Three Dimensional Heat Flow", Appl. Phys. Lett. 39, 519 (1981); L. C. Aamodt and J. C. Murphy, "Photothermal Measurements Using a Localized Excitation Source", J. Appl. Phys. 52, 4903 (1981)

(9) R. L. Thomas, L. D. Favro, K. R. Grice, L. J. Inglehart, P. K. Kuo, J. Lhota and G. Busse, "Thermal Wave Imaging for Nondestructive Evaluation", p 586, Proceedings of the 1982 IEEE Ultrasonics Symposium, B. R. McAvoy, ed., IEEE Press, New York, New York (1982)

(10) E. S. Cargill, III, "Electron-acoustic Microscopy", Physics Today, 34, 27,(1981)

(11) M. Luukkala, J. Jaarinen and A. Lehto, "Photothermal Measurement of the Thickness of Diffusion Hardened Surface Layers in Steel", Proceedings of the 1983 IEEE Ultrasonics Symposium, B. R. McAvoy, ed., IEEE Press, New York, New York (1983)

(12) Y. Martin, H. K. Wickramasinghe and E. A. Ash, "Thermo and Photo Displacement Microscopy", p 563, Proceedings of the 1982 IEEE Ultrasonics Symposium, B. R. McAvoy, ed., IEEE Press, New York, New York; L. C. M. Miranda, "Photodisplacement Spectroscopy of Solids: Theory", Appl. Optics, 22, 2882 (1983)

(13) R. G. Stearns, B. T. Khuri-Yakub and G. S. Kino, "Measurements of Thermal-Elastic Interactions with Acoustic Waves", p 595, Proceedings of the 1982 IEEE Ultrasonics Symposium, B. R. McAvoy, ed., IEEE Press, New York, New York; R. G. Stearns, B. T. Khuri-Yakub and G. S. Kino, "Phase Modulated Photoacoustics", p 649, Proceedings of the 1983 IEEE Ultrasonics Symposium, B. R. McAvoy, ed., IEEE Press, New York, New York (1983)

(14) P. K. Kuo, L. J. Inglehart, L. D. Favro and R. L. Thomas, "Experimental and Theoretical Characterization of Near Surface Cracks in Solids by Photoacoustic Microscopy", p 837, Proceedings of the 1981 IEEE Ultrasonics Symposium, B. R. McAvoy, ed., IEEE Press, New York, New York (1981)

(15) R. L. Thomas, L. D. Favro, P. K. Kuo and D. N. Rose, "Scanning Photoacoustic Microscopy of Aluminum with Aluminum Oxide, Roughness Standards and Rubber", US Army Tank-Automotive Command Research and Development Center, Warren, Michigan, Technical Report no. 12668 (1982); R. L. Thomas, L. D. Favro, P. K. Kuo, D. N. Rose, D. Bryk, M. Chaika and J. Patt, "Scanning Photoacoustic Microscopy of Aluminum with Aluminum Oxide, Roughness Standards and Rubber", US Army Tank-Automotive Command, Research and Development Center, Warren, Michigan, Technical Report No. 12957 (1984)

(16) J. L. Hunter, Acoustics, Prentice Hall (1957)

(17) Manufactured by Phrasor Scientific, Duarte, CA.

(18) K. O. Legg, Initial report of proof-of-concept study, private communication to D. N. Rose.; K. O. Legg and D. N. Rose, "Scanning Ion Acoustic Microscopy for Analyzing Ceramic Surfaces", presented at the 8th Annual Conference on Composites and Advanced Ceramic Materials, 15-18 Jan 1984, Cocoa Beach, Florida.

(19) J. K. Cochran, K. O. Legg and F. R. Baldau, "Microhardness of N-implanted Yttria Stabilized Zirconia", Proceedings of the Conference on Emergent Processing Methods in High Technology Ceramics, Raleigh, North Carolina (1982)

(20) H. S. Carslaw and J. C. Jaeger, Conduction of Heat in Solids, Oxford University Press, London (1959)

(21) R. M. White, J. Appl. Phys. 34, 3559 (1963)

(22) L. D. Favro, P. K. Kuo, M. J. Lin, L. J. Inglehart and R. L. Thomas, "A Critical Analysis of the Thermoacoustic Microscope"; F. Alan McDonald and G. C. Wetsel, Jr. "Resolution and Definition in Thermal Imaging" , Proceedings of the 1984 IEEE Ultrasonics Symposium, IEEE Press, New York, New York, to be published.

(23) J. C. Murphy, F. G. Satkiewicz and L. C. Aamodt, "Ion Acoustic Imaging of Buried Flaws in Aluminum", Review of Progress in Quantitative NDE, Vol. 5, D. O. Thompson and D. Chimenti, ed., Plenum Press, New York, New York, to be published; F. G. Satkiewicz, J. C. Murphy and L. C. Aamodt, "Ion Acoustic Imaging of Subsurface Flaws in Aluminum", presented at the 4th International Meeting on Photoacoustic, Thermal and Related Sciences, L´ Esterel, Quebec (1985), to be published in Can. J. Phys.

(24) R. S. Quimby, "Photoacoustic Microscopy with a New Modulation Technique", Appl. Phys. Lett. 39, 880 (1981); R. S. Quimby and Z. M. Liu, "Theory of Real Time Photoacoustic Microscopy", presented at the 4th International Meeting on Photoacoustic, Thermal and Related Sciences, L´ Esterel, Quebec (1985), to be published in Can. J. Phys.; H. I. Ringermacher and L. Jackman, "Deep Thermoacoustic Imaging Using Scanning Electron Acoustic Microscopy", Review of Progress in Quantitative NDE, Vol. 5, D. O. Thompson and D. Chimenti, ed., Plenum Press, New York, New York, to be published.

(25) H. F. Solnick-Legg and K. O. Legg, SBIR Phase I Rept to NSF (1983).

Distribution List

	No. of Copies
Commander, U.S. Army Tank-Automotive Command	
Warren, MI 48397-5000	
ATTN: AMSTA-R, Col J. H. Van Zandt, Jr.	1
AMSTA-RS, Mr. Don W. Rees	1
AMSTA-RSA, Dr. Grant Gerhart	1
AMSTA-RTT, Mr. Jacob Patt	1
AMSTA-QAT, Mr. Foster Brown	2
AMSTA-RCM, Mr. S. A. Catalano	1
AMSTA-RGET, Dr. Richard Munt	1
AMSTA-RGED, Dr. Walter Bryzik	1
AMSTA-RGET, Mr. John Lewakowski	1
AMSTA-TMM, Ms. Jan Dentel	1
AMSTA-TBM, Mr. William Moncrief	1
AMSTA-TSL	2
Director, U.S. Army Materials Technology Laboratory	
Watertown, MA 02171-0001	
ATTN: AMXMR-EM, Mr. Perry R. Smoot	1
AMXMR-MI, Dr. Al Broz	1
AMXMR-CO, Dr. R. N. Katz	1
AMXMR-STM, Mr. Paul Doyle	1
AMXMR-STM, Mr. Jim Kidd	1
AMXMR-MCP, Dr. George Quinn	1
AMXMR-OP, Dr. Robert E. Singler	1
AMXMR-MCP, Dr. Dennis Viechniechi	1
AMXMR-OM, Mr. Charles Gazzara	1
AMXMR-OP, Dr. James W. McCauley	1
AMXMR-OC, Dr. Janet Perkins	1
AMXMR-OP, Dr. Wensel Davidson	1
AMXMR-STQ, Mr. Fred Stinton	1
AMXMR-OM, Mr. Forrest Burns	1
SLCMT-MS, Mr. Paul W. Rolston	1
Commander, U.S. Army Research Office	
P. O. Box 12211	
Research Triangle Park, NC 27709	
ATTN: Dr. George Mayer	1
Dr. Frederick Rothwarf	1
Dr. Andrew Crowson	1
Dr. Mack Mellor	1
Commander, Naval Coastal Systems Center	
ATTN: Code 715, Mr. Steve Gorin	1
Panama City, FL 32407	

	No. of Copies
Commander, U.S. Army Mobility Equipment R&D Command ATTN: AMDME-WC (Tech Library) Fort Belvoir, VA 22060	1
Commander, Defense Technical Information Center ATTN: Bldg 5, DDAC Cameron Station Alexandria, VA 22314	12
Commander, U.S. Army Foreign Science & Technology Center ATTN: AMXST-CE Charlottesville, VA 29902	1
Commander, U.S. Army Missile Command ATTN: AMSMI-YM Redstone Arsenal, AL 35898	1
Commander, Harry Diamond Laboratories ATTN: DELHD-TD 2800 Powder Mill Road Adelphi, MD 20783	1
Dr. Robert P. Walson Cummins Engine Company, Inc. Mail Code 50165 Box 3005 Columbus, IN 47201	1
Mr. Alex Vary, Head Nondestructive Evaluation Section Materials Division MS 106-1 National Aeronautics and Space Administration Lewis Research Center 21000 Brookpark Road Cleveland, OH 44135	1
Mr. Alan R. Hirasuma L'Garde, Inc 1555 Placentia Avenue Newport Beach, CA 92663	1
Dr. David Dwight 210 Holden Hall Materials Engineering Virginia Polytechnic Institute and State University Blacksburg, VA 24061	1

	No. of Copies
Mr. John M. Corwin Research Office Chrysler Corporation P. O. Box 1118 Detroit, MI 48288	1
Mr. John E. Becker ATTN: STRBE-L U.S. Army Belvoir Research & Development Center Ft. Belvoir, VA 22060	1
Dr. Harry Ringermacher United Technologies Research Center East Hartford, CT 06108	1
Prof. John Murphy Johns Hopkins Applied Physics Laboratory The Johns Hopkins University Johns Hopkins Road Laurel, MD 20810	1
Dr. Jacob Stiglich Aerojet Ordnance Co. 2521 Michelle Drive Tustin, CA 92680	1
Dr. James M. Toth Research Center Republic Steel Corp. 6801 Brecksville Road Cleveland, OH 44135	1
Dr. Ky Narasimham Spectra Research System Bldg. 860 Vandenburg AFB, CA 93437	1
Dr. Robert V. Ieth, Chief Scientist Div. 76 Hughes Aircraft P.O. Box 902 El Segundo, CA 90245	1
Dr. Thomas J. Moran AFWAL/MLLP Wright Patterson AFB, OH 45433	1

	No of Copies
Dr. M. Srinivasan Sohio Electro Minerals Company Advanced Materials Division P.O. Box 832 Niagara Falls, NY 14302	1
Dr. David W. Oliver General Electric Bldg. 37, Rm. 251 Schenectady, NY 12345	1
Dr. Vicki Panhuise Garrett Turbine Engine Company P. O. Box 5217 Phoenix, AZ 85010	1
Dr. Pramod Khandelwal Allison Gas Turbines P. O. Box 420, Mail Stop W-5 Indianapolis, Indiana 46206	1
Mr. Dennis Hornberger Sermetel, Inc. 155 South Limerick Road Limerick, PA 19468	1
Dr. Dale Chimenti AFWAL/MLLP Wright Patterson AFB, OH 45433	1
Dr. Darryl P. Almond School of Materials Science University of Bath Cloverton Down Bath BA27AY Avon England	1
Mr. Ken Fizer Code 341 Naval Air Rework Facility Norfolk, VA 23511	1
Mr. George Lukes U.S. Army Engineering Topographical Laboratory Research Institute Ft. Belvoir, VA 22060	1

	No. of Copies
Dr. Tung-Ho Chen AMCCOM, ARDC EMD, Bldg. 3028 Dover, NJ 07801	1
Dr. Philip F. Kalina Central Research Inorganic Laboratory M.E. Pruitt Building (1776) Midland, MI 48460	1
Dr. Keith O. Legg Ionic Atlanta, Inc. 1347 Spring St., NW Atlanta, GA 30309	1
Mr. David M. Barrett Battelle Columbus Laboratories 505 King Avenue Columbus, OH 43201	1
Col Ken Grice Dept of Physics U.S. Military Academy West Point, NY 10996	1
Mr. Al Frazer, Marketing Manager Electrooptical and Data System Group P. O. Box 902 El Segundo, CA 90245	1
Commander, U.S. Army Armament, Munitions and Chemical Command Benet Weapons Laboratory Watervliet, NY 12189	
ATTN: Mr. Julius Frankel, Bldg. 115	1
Dr. M. H. Kamdar, Bldg. 115	1
Mr. Rick Campolini, SARWV-QAE, Bldg. 44	1
Mr. Henry Hartmann U.S. Army AMCCOM (D) ATTN: B19, NDT Lab Dover, NJ 07801	1
Dr. Gary F. Hawkins Aerospace Corporation MS-M2-250 P. O. Box 92957 Los Angeles, CA 90009	1

	No. of Copies
Dr. Jim Lhota Aerospace Corporation MS-M2-250 P. O. Box 92957 Los Angeles, CA 90009	1
Mr. Lewis J. Swank Ford Motor Co. Room E3172 SRL P. O. Box 2053 Dearborn, MI 48121	1
Mr. Michael Deluca PCK Technology 322 L.I.E. Drive Melville, NY	1
Mr. John Zuccon Photoacoustic Laboratory Dept. of Mechanical Engineering University of Toronto Toronto, Ontario M551A4 CANADA	1
Dr. Christopher S. Berndt NASA-Lewis Research Center MS 105-1 2100 Brookpark Road Cleveland, OH 44135	1
Dr. Andrus Niiler AMDAR-BLF (A), Bldg. 120 Ballistic Research Laboratory Aberdeen Proving Ground, MD 21005	1
Dr. Robert W. McClung Oak Ridge National Laboratory 4500-S, D-61, Box X Oak Ridge, TN 37831	1
Dr. Robert E. Richards 3M Company New Products Department 219-01-01, 3M Center St. Paul, MN 55144	1
Dr. Clay O. Ruud The Pennsylvania State University 159 Materials Research Laboratory University Park, PA 16802	1

	No. of Copies
Dr. Wayne K. Stuckey The Aerospace Corporation P. O. Box 92957, MS M2/250 Los Angeles, CA 90009	1
Dr. John B. Wachtman, Jr. Rutgers University Director, Center for Ceramics Research Room A274, P. O. Box 909 Piscataway, NJ 08854	1
Dr. James R. Wilshire Headquarters, Department of the Army ATTN: DALO-PLO Rm. 2C-556 Washington, DC 20310	1
Mr. Fred Michel AMCMT U.S. Army Material Command 5001 Eisenhower Avenue Alexandria, VA 22333	1
Mr. Mark Schumacher ATTN: MS971 Texas Instruments, Inc. 13500 N. Central Expressway Dallas, TX 75265	1
Mr. Walt Dudley Monsanto Research Corp. Mound Lab Mound Road Miamisburg, OH 45342	1
Dr. Chuck Woods Monsanto Research Corp. Mound Lab Mound Road Miamisburg, OH 45342	1
Dr. Richard S. Quimby Physics Dept. Worcester Polytechnic Institute Worcester, MA 01609	1

No. of Copies

Dr. Takehiko Kitamori 1
Energy Research Laboratory, 1168 Moriyama
Hitachi, Ibaraki
316 JAPAN

Dr. Tomoharu Watanabe 1
Department of Industrial Chemistry
Faculty of Engineering
University of Tokyo, 7-3-1 Hongo
Bunkyo-ku, Tokyo
JAPAN.113

Dr. M. Kasai 1
Department of Industrial Chemistry
Faculty of Engineering
University of Tokyo, 7-3-1 Hongo
Bunkyo-ku, Tokyo
JAPAN.113

Dr. T. Sawada 1
Department of Industrial Chemistry
Faculty of Engineering
University of Tokyo, 7-3-1 Hongo
Bunkyo-ku, Tokyo
JAPAN.113

Dr. Y. -C. Yang 1
Geo-Centers, Inc. 47 Auth Place
Suitland, MD 21014

Ms. Peg Weeks 1
McMahon Hall
Alfred University
Alfred, NY 14802

Mr. Xavier Maldague 1
National Research Council
75 de Mortagne
Boucherville, Quebec
CANADA J4B 6Y4

Mr. Eric S. Lillybeck 1
San Fernando Laboratories 10258 Norris Avenue
Pacoima, CA 91331

Manager, Defense Logistics Studies
Information Exchange
ATTN: AMXMC-D 1
Fort Lee, VA 23801

Mr. Frederick J. Dudek 1
50 UOP Plaza
Des Plaines, IL 60016-6187

Dr. Stephen T. Gonczy 1
50 UOP Plaza
Des Plaines, IL 60016-6187

Mr. Noam Arnon 1
Ceramic Materials Department
Ford Motor Company
P. O. Box 2053
Dearborn, MI 48121

Dr. David W. Richerson 1
Director, Research & Development
Ceramatec, Inc.
163 West 1700 South
Salt Lake City, Utah 84115

Dr. John Baker 1
Unviersal Energy Systems
4401 Dayton-Xenia Road
Dayton, OH 45432

Mr. Harold R. Turner 1
School of Physics
Georgia Institute of Technology
Atlanta, GA 30332